Supercontinuum Generation by Intermodal Four-Wave Mixing in a Step-Index Few-Mode Fibre

S. Perret [(a)*], G. Fanjoux [(a)], L. Bigot [(b)], J. Fatome[(c)], G. Millot [(c)], J. M. Dudley [(a)], T. Sylvestre[(a)]

[a] *Institut FEMTO-ST, Département d'Optique, CNRS, UMR 6174, Université Bourgogne Franche-Comté, Besançon, France*

[b] *Université de Lille, CNRS, UMR 8523 - PhLAM - Physique des Lasers Atomes et Molécules, Lille, France*

[c] *Laboratoire Interdisciplinaire Carnot de Bourgogne, CNRS, UMR 6303, Université Bourgogne Franche-Comté, Dijon, France*

We demonstrate broadband supercontinuum generation from 560 nm up to 2350 nm by coupling a simple Q-switched picosecond laser at 1064 nm into a normally dispersive step-index few-mode optical fiber designed to support five modes. It is further shown that multiple cascaded intermodal four-wave mixing and Raman processes occur in the fiber leading to the generation of new frequency components with far detuning up to 165 THz. The multimode properties of this fiber yield a number of intermodal nonlinear coupling terms and we compare the generated parametric sideband wavelengths from experiment with calculations from phase-matching conditions for intermodal four-wave mixing.

Introduction

The study of complex spatiotemporal dynamics of nonlinear light propagation in multimode optical fibers (MMFs) has recently witnessed renewed interest with the experimental demonstration of high-impact new phenomena in emerging key areas of laser physics and fiber optics [1,2]. Specifically, MMFs have been shown to possess specific modal properties that mediate a number of spatiotemporal nonlinear effects that are fundamentally different from those seen in standard single-mode fibers. These include the observation of multimode solitons [3], cascaded intermodal four-wave mixing (FWM) and modulation instability [4-6], geometric parametric instabilities [7], spatial beam self-cleaning [8], spin-orbit interaction [9], multimode fiber lasers [10,11] and supercontinuum (SC) generation [12-16]. The use of silica-based MMFs is advantageous to generate white-light multi-octave spanning SC spectra with large throughput in terms of power [12].

To date, most recent observations have been performed using graded-index MMFs featuring weak intermodal dispersion, although intermodal nonlinear mixing has also been reported in step-index fibers with Bessel beams [17]. In this work, we extend the study of novel nonlinear intermodal effects to step-index few-mode fibers (FMFs) to show that they can be conveniently applied to far-detuned cascaded intermodal FWM and SC generation. The main novelty of our system is to show that step-index FMFs can be combined with a simple Q-switched picosecond laser to give a multi-octave spanning supercontinuum output, as in graded-index fibers. More specifically, we experimentally demonstrate SC generation spanning

from 560 to 2350 nm by coupling a passively Q-switched microchip laser at 1064 nm into a 50-m long and 15 µm-core step-index germanium-doped silica fiber. Further experimental investigations in a shorter fiber segment show that cascaded stimulated Raman scattering and intermodal FWM effects with large frequency detuning are involved to generate the infrared and visible parts of this supercontinuum, respectively. The many FWM sidebands generated in the visible are carefully analyzed and compared with theoretical phase-matching predictions from numerical calculations of the propagation constants. The results demonstrated in this work may add a convenient and novel approach enabling efficient SC generation and far-detuned parametric conversion in few-mode step-index fibers pumped far from the zero-dispersion wavelength.

Theory

We first briefly review the theory of intermodal FWM and the main phase-matching equations relevant to this study. We consider degenerate four-wave mixing with two pump photons generating symmetrically detuned signal and idler photons [18-20]. Energy conservation yields:

$$\frac{2}{\lambda_P} = \frac{1}{\lambda_S} + \frac{1}{\lambda_I} \quad ; \quad 2\omega_P = \omega_S + \omega_I \tag{1}$$

with λ_P, λ_S and λ_I are the pump, signal and idler wavelengths, respectively. ω_P, ω_S and ω_I are their corresponding angular frequencies, and $\Omega = \omega_S - \omega_P = \omega_P - \omega_I$ is the frequency detuning between the pump and signal (idler) waves. For multimode fibers, there are two main phase-matching conditions depending on the intermodal coupling. The first involves two pump photons in two distinct linearly polarized (LP) modes, k and j [7]. This yields

$$\Delta\beta = \beta_0^{j(i)} + \beta_0^{k(s)} - \beta_0^{j(p)} - \beta_0^{k(p)} = 0, \tag{2}$$

where for instance $\beta_0^{j(p)}$ is the propagation constant of the pump wave in the j mode. The second case involves two pump photons in the same LP mode with the simpler phase-matching condition:

$$\Delta\beta = \beta_0^{j(i)} + \beta_0^{k(s)} - 2\beta_0^{l(p)} = 0. \tag{3}$$

Phase-matching in multimode fibers is achieved when the linear phase mismatch due to intermodal dispersion is compensated for by the group-velocity dispersion (GVD) and the nonlinear phase shift. The latter is generally weak compared to the two other terms and it will be neglected thereafter in the phase-matching calculations. The signal and idler wavelengths are then derived by solving the phase-matching equations (2) and (3). As we are dealing with a step-index few mode fiber, there is no direct and accurate analytical approximation of the effective indices of the LP modes, unlike for graded-index fibers [20]. The propagation constants, effective indices and GVD coefficients are obtained with finite element method (FEM)-based numerical calculations (using COMSOL software). The fiber under test was specially designed and fabricated in the FiberTech Lille platform as a bimodal fiber at 1550 nm for space-division multiplexing applications [21,22]. Specifically, it has a core diameter D=15.5 µm and a core-cladding index difference Δn=0.007. Figure 1(a) shows both the measured index profile (solid black) of the fiber and the step-index model (green dashed) used in the modal calculations. Although different, the theoretical index profile in Fig. 1(a) was set to get the exact measured values of GVD coefficients β_2 at 1550 nm for both the LP_{01} and LP_{11} modes. The simulation results for this step-index profile are plotted in Figs. 1(b-d) that respectively show the effective indices of five spatial LP modes (b), their propagation constant β (c) as well as their GVD coefficient β_2 (d).

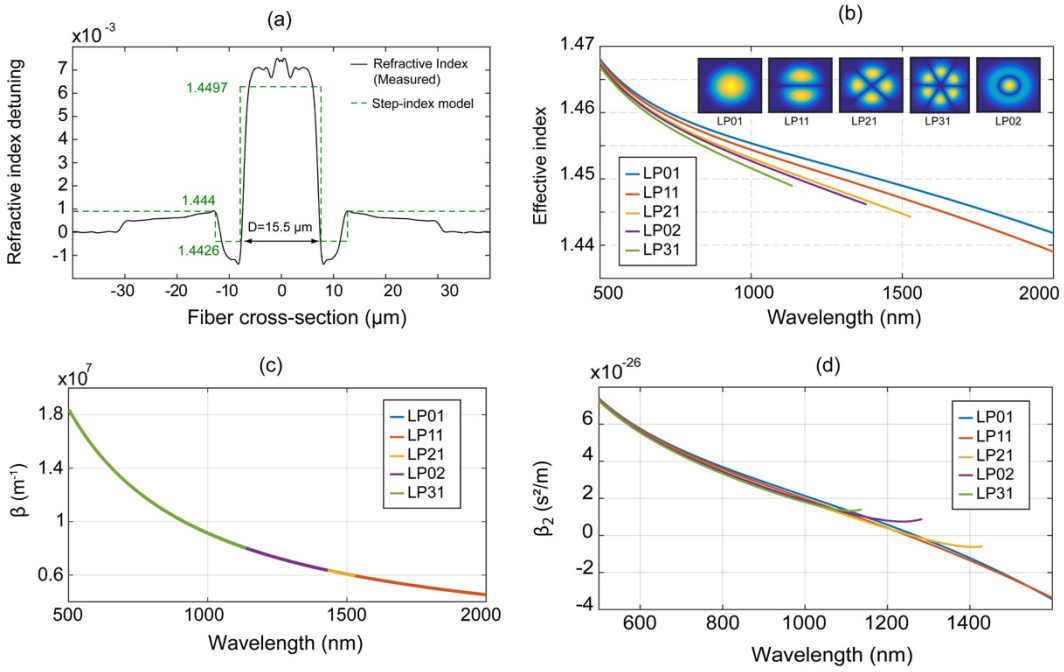

Fig. 1. (a) Refractive index profile of the step-index optical fiber used for supercontinuum generation by intermodal FWM. (b) Mode calculation results: Effective index as a function of the optical wavelength for five main spatial LP modes. The insets show the electric field amplitudes of the spatial LP modes. (c) Propagation constant and (d) group-velocity dispersion coefficient of the five modes as a function of optical wavelength.

The electric field amplitude profiles of the fundamental and higher-order LP modes are plotted in false color in inset of Fig. 1(b). At the pump wavelength of 1064 nm the fiber supports five modes, as shown in Fig. 1(b), and is characterized by a normal chromatic dispersion regime of propagation (Fig. 1(d)). Note that the curves in Figs. 1(b-d) are limited by the cut-off wavelengths of higher-order modes LP_{21}, LP_{02}, and LP_{31}, respectively. In the next section, we use these results to determine the different phase-matching conditions and compare with experiment.

Experiment

Figure 2 shows the experimental setup used to investigate SC generation and intermodal FWM. As a pump source, we used a passively Q-switched Nd:YAG microchip laser (Teemphotonics Powerchip™ series) at 1064 nm and with a repetition rate of 1 kHz and pulse duration of 600 ps (FWHM). The maximum pulse peak and average power is 80 kW and 50 mW respectively. The laser beam was injected into the fiber using a focusing lens (x10) with a 10.6 mm working distance controlled by a 3-axis translation stage. The input pump power was controlled by a variable attenuator. The output light was recorded using several optical spectral analyzers (OSA), and the modal intensity distribution of all the FWM sidebands was imaged using a CCD camera and a diffraction grating (600 lines/mm). Three different OSAs were used to cover all the wavelength range from the visible to the mid-infrared: a Yokogawa AQ6373 with a wavelength range from 350 to 1200 nm, an Agilent 86142B with a range from 600 to 1700 nm and finally an Ocean Optics NIRQUEST (NQ512-2-5) with a range from 900 up to 2500 nm. This technique also makes it possible to avoid spurious 2nd order diffraction from OSAs.

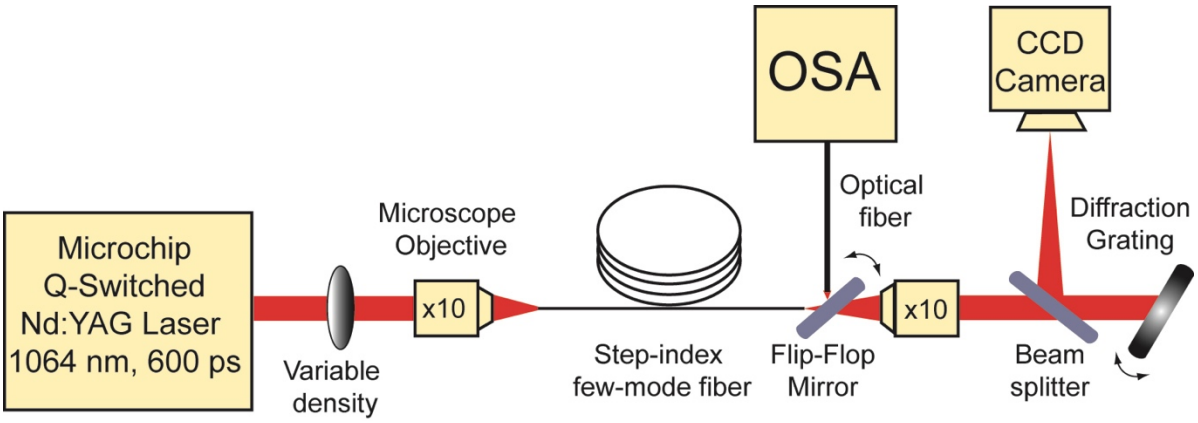

Fig. 2. Experimental setup for supercontinuum generation and intermodal FWM in a few-mode step-index fiber.

Figure 3 shows the output supercontinuum spectrum generated at a maximum coupling efficiency (26%, P_{out} = 13 mW) when pumping into both single and first higher-order mode of the fiber. The inset shows the far-field optical mode in the visible region. Note that for this fiber, the zero-dispersion wavelength is around 1300 nm (Fig. 1(d)), and so the pump wavelength is in the normal dispersion regime of the fiber. SC generation in this case arises from cascaded stimulated Raman scattering for the broadening in the infrared, and far-detuned intermodal FWM for extension towards the visible. In such pumping conditions, the SC light spans from 560 nm up 2350 nm and features several peaks in the visible, which will be discussed later. The SC spectrum and output power are relatively stable however they are extremely sensitive to the spatial injection conditions due to the multimode nature of the fiber.

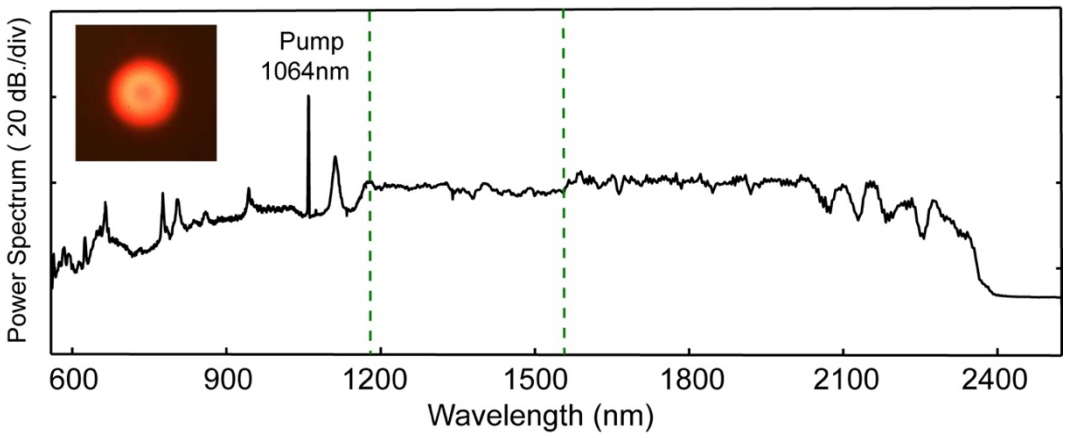

Fig. 3. Supercontinuum light spectrum experimentally generated out of 50-m long few-mode step-index fiber with a pump at 1064 nm. The average output power is 13 mW. The whole spectrum was measured by means of 3 complementary optical spectrometers to cover the whole wavelength range (the dashed lines indicate the 3 measurement ranges). The inset shows the fiber output beam in the visible.

To obtain further insight into the underlying physical mechanisms, additional experiments were performed with a shorter fiber section of 5 m. For this first case, Figure 4(a) shows the measured output spectra over the range 560-1200 nm as a function of pump power with the corresponding output far-field images of the generated parametric sidebands. As well as the pump at 1064 nm and a residue from the internal microchip CW pump at 800 nm, we see the generation of a first-order Raman Stokes line at 1110 nm (-13 THz frequency shift from the pump) and two narrow parametric sidebands at 968 nm and 1174 nm, respectively. Those sidebands are generated in the LP_{01} and LP_{11} modes by intermodal FWM involving two pump photons at 1064 nm in a mixed LP_{01}/LP_{11} mode (See image in inset). Interestingly, those two parametric sidebands are strongly enhanced by the cascaded Raman gain as they exactly match with both the second-order Stokes and anti-Stokes Raman frequency shifts (-/+ 26 THz). The parametric narrow band at 968 nm is particularly strong as it falls far from the anti-Stokes Raman absorption band. Clearly, this is the signature of a second-order Raman-assisted FWM process [23]. At higher power, both the Raman and

parametric bands significantly broaden and new FWM sidebands appear in the optical spectrum. Intermodal FWM involving the pump at 1064 nm generates a new signal at 948 nm in the LP_{11} mode and an idler at 1210 nm (not visible on Fig. 4 because of the OSA upper limit). Together with the signal at 948 nm also appear two other far-detuned parametric sidebands at 779 nm (LP_{01}) and at 667 nm (LP_{02}) by cascaded intermodal FWM. This corresponds to a frequency detuning of more than 165 THz from the initial pump frequency, almost as much as observed in graded-index multimode fibers [3].

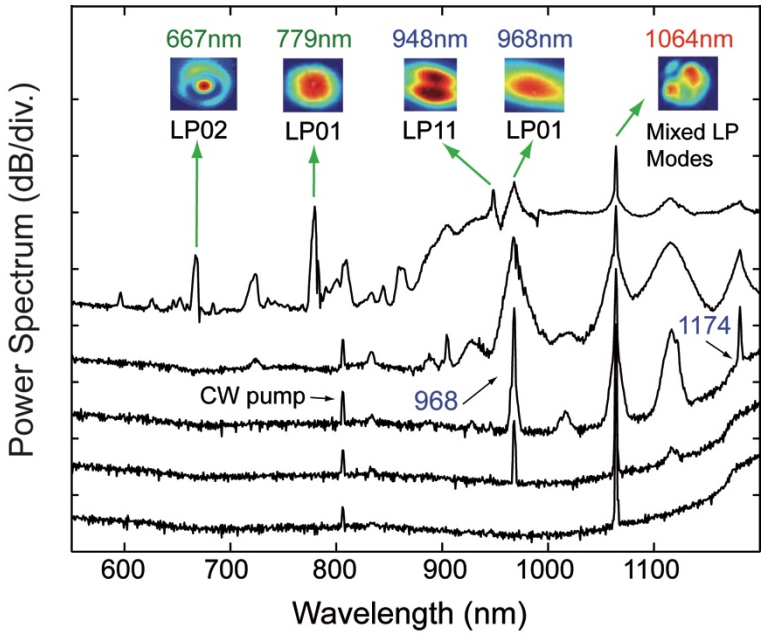

Fig. 4. Experimental output spectra for different output pump power of (from bottom to top) 0.85 mW, 1.6 mW, 2.6 mW, 3.5 mW and 8.1 mW at a fiber length of 5 m; (b). fiber output spectrum for the maximum mean power on which the FWM-wavelength and their associated LP modes are imaged with a CCD camera after passing through a diffraction grating.

We have also changed the injection conditions to preferentially excite the fundamental mode only at 1064 nm. This was achieved by replacing the microscope objective by a lens with a 25.4 mm focal length to get a beam waist of about 15 µm as large as the fiber core diameter. In such injection conditions, we recorded several output spectra from 450 nm to 1700 nm as a function of the mean pump power from 0.75 mW up to 8.4 mW. Figure 5 shows the output spectra. We still see the generation of the first-order Raman Stokes line at 1110 nm as well as the parametric sidebands at 968 nm and 1174 nm. Furthermore, two new parametric sidebands localized at 1038 nm and 1090.8 nm, that were absent in Fig. 4, can now be clearly observed near the pump wavelength. As we will see thereafter, they originate from an intermodal FWM involving the LP_{21} and LP_{02} modes. The parametric signal at 968 nm is strongly enhanced by Raman–assisted FWM as seen previously for the first pumping condition. However, none parametric sideband at 948 nm is generated in these injection conditions. Increasing further the pump

power up to 4.7 mW gives rise to two narrow parametric sidebands in the visible at 629.1 nm and 641 nm, respectively. They are in fact generated by an intermodal FWM involving the 968 nm sideband as a secondary pump wave. At higher power, Figure 5 shows that those parametric sidebands at 629.1 nm and 641 nm are strong enough to generate a Raman cascade beyond 700 nm. Note that due to the strong spectral broadening in visible region, the output mode images were not taken.

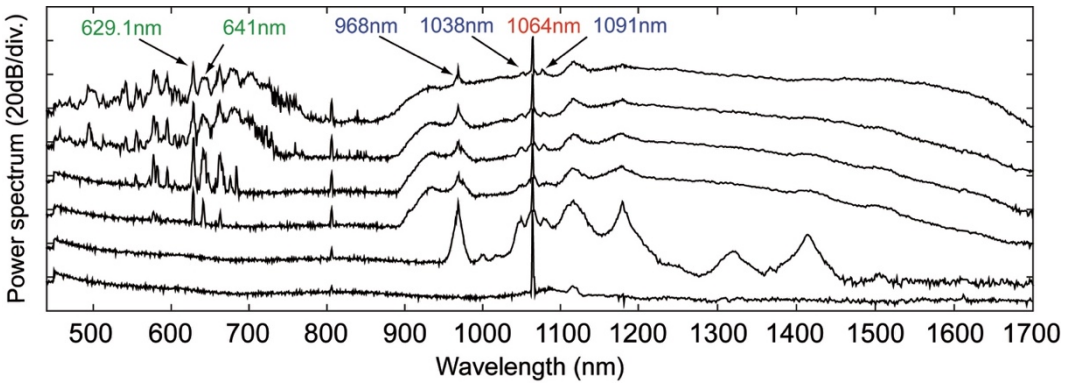

Fig. 5. Experimental spectra recorded at the output of a 5-m long segment of few-mode fiber as a function of increasing pump power (from bottom to top) 0.75 mW, 2.3 mW, 4.7 mW, 5.1 mW, 6.1 mW and 8.4 mW. The coupling conditions correspond to the fundamental mode for which the signal at 948nm wavelength is absent.

To confirm these experimental data, we have computed the phase-matching conditions using Eqs. (2) and (3) from the effective indices and the propagation constants shown in Fig. 1. This allowed us to clearly identify the main intermodal FWM processes occurring during the propagation in the optical fiber. The results are shown in Figure 6 for three cases: (a) a pump wave at 1064 nm in a mixed mode configuration; a secondary pump at 948 nm in the LP_{11} mode and (c) a secondary pump at 968 nm in the LP_{01} mode. All phase-matching curves in Fig. 6 correspond to different intermodal couplings listed in the right captions. In addition, the resulting predictions of phase-matched signal wavelength are indicated with black dashes while the experimental data are reported in red for the sake of comparison. Note that some of the phase-matching curves are also limited due to the cut-off of higher-order modes.

As can be seen in Fig. 6(a) for the main pump at 1064 nm, there is a pretty good agreement between the experiment data and the theory in black for the three main parametric sidebands at 948 nm in LP_{11} mode, 968 nm in LP_{01} mode and 1038.5 nm in the LP_{21} mode. The small discrepancies could be attributed to the errors in modelling the exact step-index profile of the fiber and, in particular, the higher-order dispersion terms that play a significant role in the phase-matching conditions for large frequency detuning, as recently shown in Ref. [5]. In Fig. 6(b) we have displayed the phase-matching curves for a secondary pump at 948 nm in the LP_{11} mode, which appears only in the first experimental spectra shown in Fig. 4.

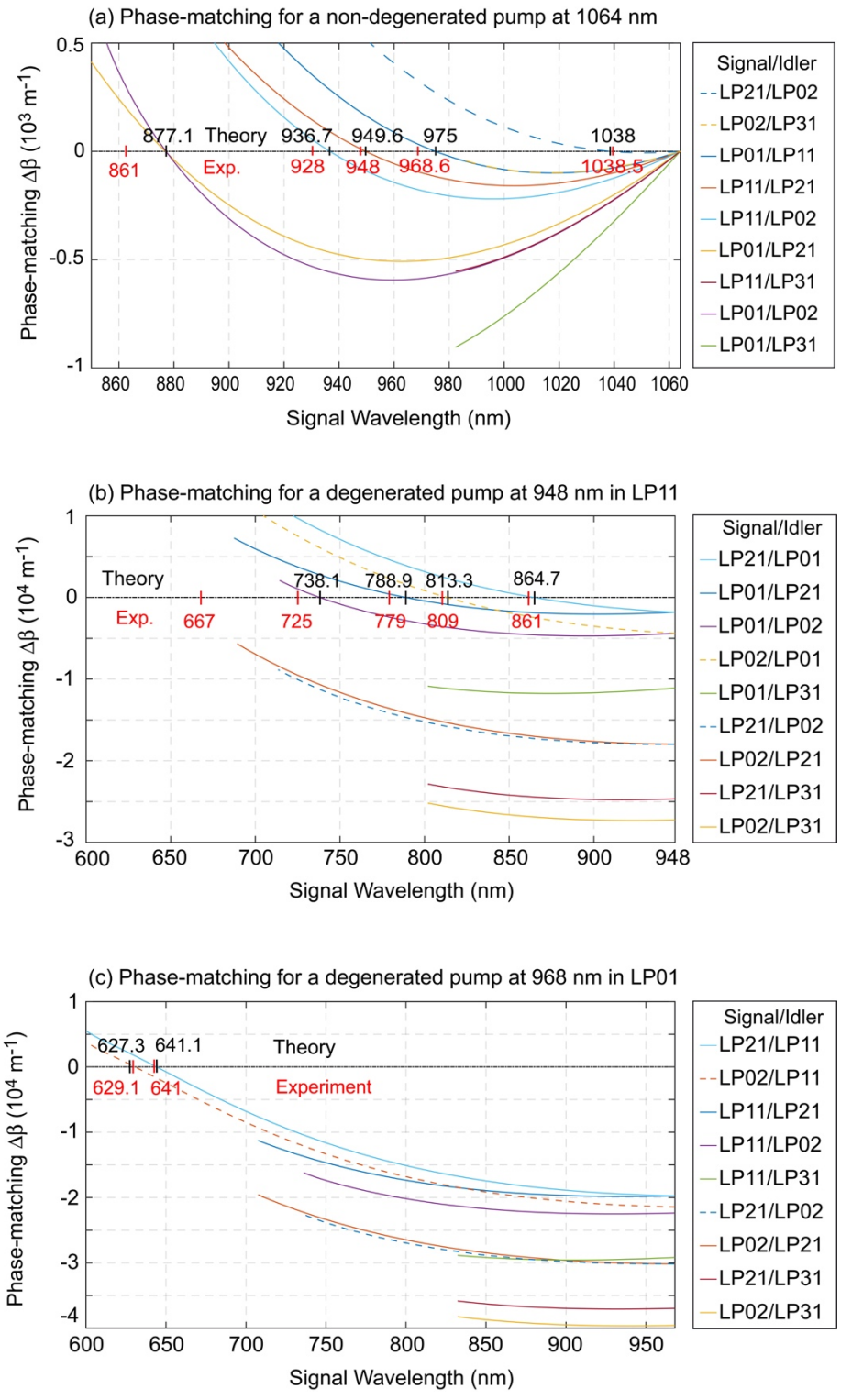

Fig. 6. Calculated intermodal phase-matching conditions as a function of signal wavelength for three different pump wavelengths and modal interactions shown in right insets. (a) Main pump at 1064 nm (b) Secondary pump at 948 nm and (c) Secondary pump at 968 nm. Black dashes depict for the calculated signal wavelengths while red dashes display the experimental data.

Once again there is a good match between experiment in red and theory in black as the parametric sidebands at 725 nm and 779 nm fall rather close to the theoretical values. If we now have a look at the phase-matching curves in Fig. 6 (c) for a secondary pump at 968 nm in the LP_{01} mode, we also found a good agreement for visible FWM sidebands at 629.1 nm and 641 nm. Since the parametric sideband at 968 nm is generated preferentially in the fundamental LP_{01} mode, it becomes strong enough to act as a secondary pump, giving rise to the visible sidebands at 629.1 nm and 641 nm by intermodal FWM [3,7]. In a similar way, the parametric sideband pump at 948 nm in LP_{11} mode plays the role of a secondary pump that generates the FWM sideband at 667 nm in LP_{02} mode, as shown experimentally in Fig. 4 and theoretically in Fig. 6(b). To confirm the role of this secondary pump, we must take into account the idler wavelength and its modal distribution. In this case, the idler wave for a signal at 667 nm in LP_{02} is expected at 1638 nm in the LP_{21} mode. Since the fiber was designed to be bimodal (LP_{01} and LP_{11}) at 1550 nm however, the LP_{21} mode is not guided at 1658 nm and this idler sideband cannot be observed experimentally. Table 1 below summarizes the phase-matching calculations and comparison with all experimental data. As can be seen the agreement is satisfactory, confirming the main intermodal FWM processes that occur in the step-index few-mode fiber. Note however that most of the calculated idler sidebands are absent in the experimental spectra of Figs. 3 and 6 since they are buried in the continuum.

Table 1: Comparison between theory and experiment of phase-matched signal and idler wavelengths for three pump configurations.

Phase-matching Calculations	Theory		Experiment	
Pump configuration	Pump Wavelength at 1064 nm			
Spatial Modes [LP_{xx}]	Signal Wavelength	Idler Wavelength	Signal Wavelength	Idler Wavelength
LP_{01}/LP_{11}	975 nm	1170 nm	968 nm	1174 nm
LP_{11}/LP_{21}	950 nm	1208 nm	948 nm	1210 nm
LP_{21}/LP_{02}	1038 nm	1091.3 nm	1038.5 nm	1090.8 nm
LP_{11}/LP_{02}	936.7 nm	1231 nm	928 nm	1246 nm
Pump configurations	Pump Wavelength at 948 nm in LP_{11}			
LP_{02}/LP_{21}			667 nm	1638 nm*
LP_{01}/LP_{21}	789 nm	1187 nm	779 nm	1210 nm
LP_{01}/LP_{02}	738 nm	1324 nm	725 nm	1369 nm*
Pump configuration	Pump Wavelength at 968 nm in LP_{01}			
LP_{21}/LP_{11}	641.1 nm	1975.1 nm	641 nm	1976 nm*
LP_{02}/LP_{11}	627.3 nm	2118.7 nm	629.1 nm	2098.4nm*

*Those idler wavelengths have been calculated from the experimental signal wavelengths.

Conclusion

To conclude we have reported in this work on the experimental generation of supercontinuum spanning two octaves from 560 to 2350 nm in a step-index few-mode fiber pumped with a Q-switched microchip laser at 1064 nm. We have clearly identified the spectral broadening arising from both cascaded Raman scattering and intermodal nonlinear four-wave mixing processes. These results highlight the fact that wideband fiber-based SC generation can be achieved in the normal dispersion regime without involving solitons and dispersive wave generation. Moreover, a good agreement has been obtained between our theoretical predictions based on phase-matching conditions of intermodal FWM and experimental observations of generated FWM sidebands. We anticipate that the results demonstrated in this work may provide a convenient and novel approach enabling efficient SC generation far from the zero-dispersion wavelength of optical fibers, and may stimulate new possibilities for technological applications of multimode and few-mode fibers. A new orientation of this field with different materials and waveguides such as silicon nitride (SiN) chip has received recent attention [24].

Acknowledgements

This project has received funding from the European union H2020 program MSCA-ITN-SUPUVIR under grant agreement 722380, the Labex ACTION (ANR-11-LABX-0001-01), and the I-SITE BFC Program (ANR-15-IDEX-0003), and the Conseil Régional de Bourgogne Franche-Comté. The authors thank V. Pecheur, A.N. Ghosh, C. Lechevalier, L Gauthier-Manuel, A. Mosset, and C. Billet for technical support.

References

[1] L. G. Wright, D. N. Christodoulides, F. W. Wise, “Controllable spatiotemporal nonlinear effects in multimode fibres,” Nat. Photon. 9, 306 (2015).

[2] L. G. Wright et al., "Multimode Nonlinear Fiber Optics: Massively Parallel Numerical Solver, Tutorial, and Outlook," in IEEE Journal of Selected Topics in Quantum Electronics, vol. 24, no. 3, pp. 1-16, May-June 2018.

[3] Z. Zhu, L. G. Wright, D. N. Christodoulides and F. W. Wise, “Observation of multimode solitons in few-mode fiber” Opt. Lett. 41, 4819 (2016).

[4] R. Dupiol, A. Bendahmane, K. Krupa, A. Tonello, M. Fabert, B. Kibler, T. Sylvestre, A. Barthelemy, V. Couderc, S. Wabnitz, and G. Millot, “Far-detuned cascaded intermodal four-wave mixing in a multimode fiber,” Opt. Lett. 42, 1293 (2017).

[5] A. Bendahmane, K. Krupa, A. Tonello, D. Modotto, T. Sylvestre, V. Couderc, S. Wabnitz, and G. Millot, "Seeded intermodal four-wave mixing in a highly multimode fiber," J. Opt. Soc. Am. B 35, 295-301 (2018).

[6] R. Dupiol, A. Bendahmane, K. Krupa, J. Fatome, A. Tonello, M. Fabert, V. Couderc, S. Wabnitz, and G. Millot, "Intermodal modulational instability in graded-index multimode optical fibers," Opt. Lett. 42, 3419-3422 (2017).

[7] K. Krupa, A. Tonello, A. Barthelemy, V. Couderc, B. M. Shalaby, A. Bendahmane, G. Millot, and S. Wabnitz, “Observation of Geometric Parametric Instability Induced by the Periodic Spatial Self-Imaging of Multimode Waves.” Phys. Rev. Lett. 116, 183901 (2016).

[8] K. Krupa, A. Tonello, B. M. Shalaby, M. Fabert, A. Barthelemy, G. Millot, S. Wabnitz, and V. Couderc, “Spatial beam self-cleaning in multimode fibres,” Nat. Photon. 11, 237 (2017).

[9] L. P. Vitullo and C. C. Leary, and P. Gregg and R. A. Smith, and D. V. Reddy and S. Ramachandran, M. G. Raymer, “Observation of Interaction of Spin and Intrinsic Orbital Angular Momentum of Light,” Phys. Rev. Lett. 118, 8, 083601, (2017).

[10] L. G. Wright, D. N. Christodoulides, and F. W. Wise, “Spatiotemporal mode-locking in multimode fiber lasers,” Science 358, 94 (2017).

[11] R. Guenard, K. Krupa, R. Dupiol, M. Fabert, A. Bendahmane, V. Kermene, A. Desfarges-Berthelemot, J. L. Auguste, A. Tonello, A. Barthélémy, G. Millot, S. Wabnitz, and V. Couderc, “Nonlinear beam self-cleaning in a coupled cavity composite laser based on multimode fiber”, Opt. Express 25, 22219 (2017).

[12] M. A. Eftekhar, L. G. Wright, M. S. Mills, M. Kolesik, R. A. Correa, F. W. Wise and D. N. Christodoulides, “Versatile supercontinuum generation in parabolic multimode optical fibers,” Opt. Exp. **25**, 9078 (2017).

[13] K. Krupa, C. Louot, V. Couderc, M. Fabert, R. Guenard, B. M. Shalaby, A. Tonello, A. Barthélémy, D. Pagnoux, P. Leproux, A. Bendahmane, R. Dupiol, G. Millot, S. Wabnitz, "Spatiotemporal Characterization of Supercontinuum Extending from the Visible to the Mid-Infrared in Multimode Graded-Index Optical Fiber," Opt. Lett. **41**, 5785-5788 (2016).

[14] C. Lesvigne, V. Couderc, A. Tonello, P. Leproux, A. Barthélémy, S. Lacroix, F. Druon, P. Blandin, M. Hanna, and P. Georges, "Visible supercontinuum generation controlled by intermodal four-wave mixing in microstructured fiber," Opt. Lett. **32**, 2173-2175 (2007).

[15] Arnaud Mussot, Thibaut Sylvestre, Laurent Provino, and Hervé Maillotte, "Generation of a broadband single-mode supercontinuum in a conventional dispersion-shifted fiber by use of a subnanosecond microchiplaser," Opt. Lett. **28**, 1820-1822 (2003).

[16] F. Poletti and P. Horak, "Dynamics of femtosecond supercontinuum generation in multimode fibers," *Opt. Express*, vol. 17, no. 8, pp. 6134–6147, Apr. 2009.

[17] J. Demas, P. Steinvurzel, B. Tai, L. Rishoj, Y. Chen and S. Ramanchandran, "Intermodal nonlinear mixing with Bessel beams in optical fiber," Optica Vol. 2, 14 (2015).

[18] G. P. Agrawal, "Nonlinear Fiber Optics", Fifth Edition, Academic Press, ISBN-978-0-12397-023-7 (2013).

[19] R. H. Stolen, "Phase-matched three-wave mixing in silica fiber optical waveguides," *Appl. Phys. Lett.*, vol. 24, no. 7, pp. 2195–2198, Oct. 1974.

[20] E. Nazemosadat, H. Pourbeyram, and A. Mafi, "Phase matching for spontaneous frequency conversion via four-wave mixing in graded index multimode optical fibers," J. Opt. Soc. Am. B **33**, 144-150 (2016).

[21] D. J. Richardson, J. M. Fini, and L. E. Nelson, "Space-division multiplexing in optical fibres," Nature Photon. **7**, pp. 354–362, Apr. 2013.

[22] C. C. Castineiras Carrero, G. Le Cocq, B. Sévigny, L. Bigot, A. Le Rouge, Y. Quiquempois, M. Bigot-Astruc, D. Molin, and P. Sillard, "Using advanced S2 analysis to measure mode coupling in a 2-LP-Mode Fiber," in *Optical Fiber Communication Conference*, OSA Technical Digest (online) (Optical Society of America, 2016), paper W4F.5.

[23] T. Sylvestre, H. Maillotte, E. Lantz, and P. Tchofo Dinda, "Raman-assisted parametric frequency conversion in a normally dispersive single-mode fiber," Opt. Lett. 24, 1561-1563, (1999).

[24] S. Signorini, M. Mancinelli, M. Borghi, M. Bernard, M. Ghulinyan, G. Pucker, and L. Pavesi, "Intermodal Four Wave Mixing in Silicon waveguides," Photonics Research, 6, 8, (2018).

Note: This is an example of a footnote to the title if the paper was part of a conference: Contributed paper, published as part of the Proceedings of the 17th International Conference on Physics, Anytown, State, May 2010.

1. This is an example of a footnote to an author's name: Author to whom correspondence should be addressed. Electronic mail: author@somewhere.org.

b) This research was performed while B. Author was at Anywhere National Laboratory, City, State, Postal code, Country.

c) B. Author and C. Author contributed equally to this work.